

UNIVERSITY OF BIRMINGHAM

Research at Birmingham

Aldebaran b's temperate past uncovered in planet search data

Farr, Will; Pope, Benjamin J. S.; Davies, Guy; North, Thomas; White, Timothy R.; Barrett, Jim W.; Miglio, Andrea; Lund, Mikkel; Antoci, Victoria; Andersen, Mads Fredslund; Grundahl, Frank; Huber, Daniel

DOI:

[10.3847/2041-8213/aadfde](https://doi.org/10.3847/2041-8213/aadfde)

License:

Other (please provide link to licence statement)

Document Version

Publisher's PDF, also known as Version of record

Citation for published version (Harvard):

Farr, WM, Pope, BJS, Davies, GR, North, TSH, White, TR, Barrett, JW, Miglio, A, Lund, MN, Antoci, V, Andersen, MF, Grundahl, F & Huber, D 2018, 'Aldebaran b's temperate past uncovered in planet search data', *The Astrophysical Journal*, vol. 865, no. 2, L20. <https://doi.org/10.3847/2041-8213/aadfde>

[Link to publication on Research at Birmingham portal](#)

Publisher Rights Statement:

Checked for eligibility: 23/10/2018

The final version of record can be found at:

<https://doi.org/10.3847/2041-8213/aadfde>

General rights

Unless a licence is specified above, all rights (including copyright and moral rights) in this document are retained by the authors and/or the copyright holders. The express permission of the copyright holder must be obtained for any use of this material other than for purposes permitted by law.

- Users may freely distribute the URL that is used to identify this publication.
- Users may download and/or print one copy of the publication from the University of Birmingham research portal for the purpose of private study or non-commercial research.
- User may use extracts from the document in line with the concept of 'fair dealing' under the Copyright, Designs and Patents Act 1988 (?)
- Users may not further distribute the material nor use it for the purposes of commercial gain.

Where a licence is displayed above, please note the terms and conditions of the licence govern your use of this document.

When citing, please reference the published version.









Take down policy

While the University of Birmingham exercises care and attention in making items available there are rare occasions when an item has been uploaded in error or has been deemed to be commercially or otherwise sensitive.

If you believe that this is the case for this document, please contact UBIRA@lists.bham.ac.uk providing details and we will remove access to the work immediately and investigate.



Aldebaran b's Temperate Past Uncovered in Planet Search Data

Will M. Farr^{1,2,3} , Benjamin J. S. Pope^{4,5,9} , Guy R. Davies^{2,6} , Thomas S. H. North^{2,6}, Timothy R. White⁶ ,
Jim W. Barrett^{1,2}, Andrea Miglio^{2,6} , Mikkel N. Lund^{2,6} , Victoria Antoci⁶ , Mads Fredslund Andersen⁶,
Frank Grundahl⁶ , and Daniel Huber^{4,6,7,8}

¹ Birmingham Institute for Gravitational Wave Astronomy, University of Birmingham, Birmingham B15 2TT, UK; farr@bham.ac.uk

² School of Physics and Astronomy, University of Birmingham, Birmingham B15 2TT, UK

³ Center for Computational Astrophysics, Flatiron Institute, 162 Fifth Avenue, New York, NY 10010, USA

⁴ Sydney Institute for Astronomy (SIfA), School of Physics, University of Sydney, NSW 2006, Australia

⁵ Center for Cosmology and Particle Physics, Department of Physics, New York University, 726 Broadway, New York, NY 10003, USA

⁶ Stellar Astrophysics Centre, Department of Physics and Astronomy, Aarhus University, Ny Munkegade 120, DK-8000 Aarhus C, Denmark

⁷ Institute for Astronomy, University of Hawai'i, 2680 Woodlawn Drive, Honolulu, HI 96822, USA

⁸ SETI Institute, 189 Bernardo Avenue, Mountain View, CA 94043, USA

Received 2018 February 23; revised 2018 August 8; accepted 2018 August 12; published 2018 September 27

Abstract

The nearby red giant Aldebaran is known to host a gas giant planetary companion from decades of ground-based spectroscopic radial velocity measurements. Using Gaussian Process-based Continuous Auto-Regressive Moving Average models, we show that these historic data also contain evidence of acoustic oscillations in the star itself, and verify this result with further dedicated ground-based spectroscopy using the SONG telescope and space-based photometry with the *Kepler Space Telescope*. From the frequency of these oscillations we determine the mass of Aldebaran to be $1.16 \pm 0.07 M_{\odot}$, and note that this implies its planet will have been subject to insolation comparable to the Earth for some of the star's main sequence lifetime. Our approach to sparse, irregularly sampled time series astronomical observations has the potential to unlock asteroseismic measurements for thousands of stars in archival data, and push to lower-mass planets around red giant stars.

Key words: methods: data analysis – methods: statistical – planets and satellites: individual (Aldebaran b) – stars: individual (Aldebaran) – stars: oscillations (including pulsations) – techniques: radial velocities

Supporting material: data behind figures

1. Introduction

Aldebaran (α Tauri) is a well-known first-magnitude red giant star, and has long been the subject of astronomical investigations. It was one of the first stars around which an extrasolar planet candidate was identified, by looking for Doppler shifts from the star's reflex motion around the common center of mass with its companion (the radial velocity (RV) method; Struve 1952). While the hot Jupiter 51 Peg b (Mayor & Queloz 1995) was the first exoplanet to be recognized as such, before this, Hatzes & Cochran (1993) had noted RV variations in Pollux (β Gem; subsequently confirmed as a planet: Hatzes et al. 2006; Han et al. 2008), Arcturus (α Boo; unconfirmed), and Aldebaran. After further investigation by Hatzes & Cochran (1998), Hatzes et al. (2015) have now claimed a firm RV detection of a planetary-mass companion Aldebaran b, with a period of 629.96 ± 0.90 days.

In this Letter, we present a re-analysis of these original RV data in which we not only confirm the planetary signal, but detect acoustic oscillations in Aldebaran for the first time. Hatzes & Cochran (1993) noted night-to-night RV variability: this is the noise floor limiting the sensitivity to sub- M_J planets around giants in RV surveys (Sato et al. 2005; Jones et al. 2014). We pull out the asteroseismic signal in this planet-hunting noise. We validate this method and its result with new independent RV observations with the Hertzprung SONG Telescope, and photometry from the *K2* Mission. By measuring the frequency of maximum power of these p -mode oscillations, ν_{\max} , we asteroseismically determine the mass of

Aldebaran to be $1.16 \pm 0.07 M_{\odot}$. This precise stellar mass allows us to calculate that Aldebaran b and any satellites it may have, although they are now likely to be very hot, would have had equilibrium temperatures comparable to that of the Earth when Aldebaran was on the main sequence. It is possible that they may have once been habitable, billions of years ago.

Our new approach to asteroseismic data analysis, based on Continuous Auto-Regressive Moving Average (CARMA) models, can extract exoplanet signals together with measures of ν_{\max} from sparse and irregularly sampled time series. Studies of small numbers of planet-hosting giants to determine their asteroseismic parameters ordinarily require dedicated observing campaigns with hundreds or thousands of epochs (Stello et al. 2017). An all-sky survey to find planetary companions and to precisely measure the masses of all nearby red giant stars is feasible with this new approach, and the required data either already exist in large RV exoplanet surveys, or are easy to obtain with ground-based telescopes.

2. Asteroseismology of Red Giants

Asteroseismology is a powerful tool for the characterization of red giant stars (see Chaplin & Miglio 2013; Hekker & Christensen-Dalsgaard 2017, for detailed reviews). Red giants exhibit oscillations that are excited and damped by stellar convection. In the power spectrum of either RV or photometric observations, these modes of oscillation form a characteristic pattern of peaks that can be used to infer intrinsic stellar properties (e.g., Davies & Miglio 2016). The easiest properties of the pattern to determine are the frequency of maximum amplitude ν_{\max} and

⁹ NASA Sagan Fellow.

the so-called large separation $\Delta\nu$ (Kjeldsen & Bedding 1995), which are often referred to as global asteroseismic parameters.

These parameters can be used to estimate the radius R , mass M , and surface gravity g of stars when combined with an estimate of the effective temperature T_{eff} through scaling relations

$$\left(\frac{R}{R_{\odot}}\right) \simeq \left(\frac{\nu_{\text{max}}}{\nu_{\text{max},\odot}}\right) \left(\frac{\Delta\nu}{\Delta\nu_{\odot}}\right)^{-2} \left(\frac{T_{\text{eff}}}{T_{\text{eff},\odot}}\right)^{0.5}, \quad (1)$$

$$\left(\frac{M}{M_{\odot}}\right) \simeq \left(\frac{\nu_{\text{max}}}{\nu_{\text{max},\odot}}\right)^3 \left(\frac{\Delta\nu}{\Delta\nu_{\odot}}\right)^{-4} \left(\frac{T_{\text{eff}}}{T_{\text{eff},\odot}}\right)^{1.5}, \quad (2)$$

$$\left(\frac{g}{g_{\odot}}\right) \simeq \left(\frac{\nu_{\text{max}}}{\nu_{\text{max},\odot}}\right) \left(\frac{T_{\text{eff}}}{T_{\text{eff},\odot}}\right)^{0.5}. \quad (3)$$

The accuracy of these scaling relations is still a matter of ongoing work, but recent comparisons using *Gaia* parallaxes have shown encouraging agreement for red giants (e.g., Huber et al. 2017; Zinn et al. 2018). Viani et al. (2017) recently used models to demonstrate that the ν_{max} scaling relation may show a dependence on the mean molecular weight. However, this effect is typically at the 0.01–0.02 dex level for red giants, which is a factor ~ 2 – 4 smaller than our measurement uncertainties (see Section 4) and thus does not significantly affect the conclusions in this Letter.

The ability to measure ν_{max} and $\Delta\nu$ depends on the length and sampling rate of a data set. In practice, for the higher luminosity red giants it is more straightforward to measure ν_{max} than $\Delta\nu$. Typical values for ν_{max} range from 0.1 to 20 μHz for luminous giants and 20–50 μHz for stars near the red clump. For the evolutionary stages, $\Delta\nu$ typically ranges from 0.02–3 μHz and 3–7 μHz depending on stellar mass and T_{eff} (e.g., Mosser et al. 2011, 2013). Hence, ν_{max} requires less frequency resolution than $\Delta\nu$ to establish a good measurement.

3. Time-domain Models

RV variations intrinsic to the star, such as those caused by stellar oscillations, have previously limited the precision with which red giant planets have been studied (Sato et al. 2005). We aim to model these noise processes and use them to recover asteroseismic information, as well as to improve our estimates of the orbital parameters of the planet. It is easy to observe Aldebaran and similarly bright stars with ground-based spectroscopic instruments, typically only requiring short exposures that can be obtained even under adverse observing conditions. There is indeed a considerable archive of such observations already, as a legacy of RV surveys conducted to find exoplanets. In most cases so far, however, these have not been useful for asteroseismology because these RV data are sparsely and irregularly sampled. Because we have to pause observations during the day, during poor weather conditions, or simply when targets of higher priority are being observed, we get time series that may have significant and uneven gaps. This introduces a window-function effect: the power spectrum as constructed, for example, by a Fourier transform, or a Lomb–Scargle Periodogram (Lomb 1976; Scargle 1982), is convolved with the Fourier transform of the window function, introducing strong sidelobes adjacent to real frequency peaks and causing crosstalk between adjacent frequency channels. This imposes significant limitations both on the signal-to-noise and frequency resolution of power spectra derived from linear

methods such as the Lomb–Scargle periodogram, and in practice makes asteroseismology with these conventional approaches difficult or impossible from the ground for stars with oscillation periods ranging from ~ 12 hr to \sim a few days.

This situation can be improved if we apply nonlinear statistical inference methods. Brewer & Stello (2009) show that a system of driven, damped harmonic oscillators such as we encounter in asteroseismology can be statistically modeled as a Gaussian Process (GP), with a covariance kernel consisting of a sum of damped sinusoids. The hyperparameters of this process encode features of the power spectral density distributions and are insensitive to the window function. GPs with quasi-periodic kernels have previously been used to re-analyze RV data for main sequence stars (Haywood et al. 2014; Rajpaul et al. 2015), where the noise is from stellar activity, but have not previously been applied to red giant asteroseismology. Unfortunately, these methods are impractical for long time series, as the computational cost of evaluating the standard GP likelihood function scales as $\mathcal{O}(n^3)$.

Fortunately, the damped and driven harmonic oscillator GP can be written as the solution of a class of stochastic ordinary differential equations, the CARMA models, whose likelihoods can be evaluated in linear time. For problems such as this, we have access to these powerful computational tools for inferring their power spectral densities. Our treatment of CARMA models is described more fully in Appendix A. Kelly et al. (2014) also gave more details on CARMA processes in an astronomical context. They showed how a state-space model of the process $y(t)$ can be tracked through a time series of uncertain observations $y_k = y(t_k) + \epsilon_k$, with Gaussian noise ϵ_k of zero mean and known (heteroskedastic) variance, using a Kalman filter to produce a likelihood function $p(y_k | \sigma, r_i, b_j)$ depending on the amplitude of the stochastic forcing, σ , the (possibly complex) eigenfrequencies of the ordinary differential equation (ODE), r_i , and parameters describing the power spectrum of the stochastic forcing, b_j in $\mathcal{O}(n)$ computational time. Foreman-Mackey et al. (2017) has demonstrated that the same model can also be implemented via a novel matrix factorization, and demonstrated its asteroseismic potential modeling the light curve of KIC 11615890.

Here we have adopted the Kelly et al. (2014) approach. The CARMA.jl package¹⁰ implements Kalman filters that can compute the likelihood of a set of observations parameterized by either the r_i and b_j or the rms amplitudes A_i of each eigenmode of the ODE and the corresponding roots r_i . This likelihood is computed for the residuals of a deterministic Keplerian RV mean model for the planetary companion. Because we have a set of observations taken with different instruments at different sites (see Section 4.1), we include RV offset (i.e., mean value) parameters that are instrument- and site-dependent, and also an instrument- and site-dependent uncertainty scaling parameter. Thus, the i th RV measured at site and instrument combination j , y_{ij} , is assumed to be

$$y_{ij} = v_r(t_i) + \mu_j + y(t_i) + \nu_j \epsilon_{ij}, \quad (4)$$

where t_i is the time of the measurement, v_r is the planetary RV signal, μ_j is the mean RV offset for site and instrument combination j , $y(t)$ is the CARMA process representing stellar activity, ν_j is the uncertainty scaling parameter for site and instrument combination j , and ϵ_{ij} is an independent Gaussian

¹⁰ <https://github.com/farr/CARMA.jl>

Table 1
The Parameters in Our Model Equation (4) and Their Priors

Parameter	Prior	Description
Site/Instrument RV Offset and Uncertainty Scaling		
μ_j	$N(\langle y_j \rangle, 10\sigma_{y_j})(\mu_j)^a$	The site/instrument RV offset
ν_j	$1/\nu_j, \nu_j \in [1/2, 2]$	The site/instrument uncertainty scale factor
Keplerian Parameters		
K	$1/K, K \in [\min_j \sigma_{y_j}/100, \max_j 10\sigma_{y_j}]$	RV semi-amplitude
P	$1/P, P \in [600, 700]$ days	Keplerian period
e	$2e, 0 \leq e < 1^b$	Keplerian eccentricity
ω	const, $0 \leq \omega < 2\pi$	Longitude of pericenter
χ	const, $0 \leq \chi < 1$	Pericenter passage is at $t = \chi P$
CARMA Parameters		
A_k	$1/A_k, A_k \in [\min_j \sigma_{y_j}/100, \max_j 10\sigma_{y_j}]$	rms amplitude of stochastic mode
r_k	$1/r_k, \Re r_k \in [1/(2T), 0.05 \mu\text{Hz}], \Im r_k = 0^c$	The damping rates for real modes
f_k	$1/f_k, f_k \in [0.1, 10] \mu\text{Hz}$	The frequency of oscillatory modes
Q_k	$1/Q_k, Q_k \in [1, 1000]$	The quality factor of oscillatory modes

Notes. Site and instrument combinations are indexed by j . Modes in the stochastic process are indexed by $k \in [1, p]$ and are either real (parameterized by a rate parameter r_k) or complex (parameterized by a frequency f_k and quality factor Q_k).

^a $\langle y_j \rangle$ and σ_{y_j} are the mean and standard deviation of the RV time series from site and instrument combination j .

^b We actually sample in and impose a (flat) prior on $x \equiv e \cos \omega$ and $y \equiv e \sin \omega$.

^c Here T is the time span of the measurements over all sites.

random variable with mean zero and standard deviation equal to the quoted uncertainty of the observation. We impose broad priors (see Table 1) on the parameters of the planetary RV signal, the CARMA process, the μ_j offsets, and the ν_j scale factors. We treat the frequency of maximum asteroseismic power, ν_{\max} , as the frequency of an appropriate eigenmode in the CARMA process representing the stellar activity; this is equivalent to fitting a Lorentzian profile to a set of unresolved asteroseismic modes. We used the nested sampling algorithm of the `Ensemble.jl` package¹¹ to calculate the marginal likelihood (evidences) and draw samples from the posterior distribution over the parameters of our various models.

4. Aldebaran

Aldebaran is a red giant star with spectral type K5, one of the nearest such stars at a distance of only 19.96 ± 0.38 pc as determined by *Hipparcos* (van Leeuwen 2007). Its position near the Ecliptic permits the determination of its angular diameter by lunar occultations and by interferometry (20.58 ± 0.03 mas; Beavers & Eitter 1979; Brown et al. 1979; Panek & Leap 1980; Richichi & Roccatagliata 2005). These tight constraints are valuable in breaking degeneracies in stellar modeling and make this an ideal star for asteroseismic characterization (Appendix C).

4.1. Archival Observations

Hatzes et al. (2015) reported on RV observations of Aldebaran from the coudé échelle spectrograph of the Thüringer Landessternwarte Tautenburg, the Tull Spectrograph of the McDonald

2.7 m telescope, and the Bohyunsan Observatory Échelle Spectrograph spectrograph of the Bohyunsan Optical Astronomy Observatory spanning the period from 2000.01 to 2013.92. Combined with earlier observations (Hatzes & Cochran 1993), we construct a full time series spanning more than two decades from 1980.80 to 2013.71 (Figure 1) and fit this with a Keplerian model and a CARMA process. We find evidence for a low-quality ($Q = 2.1_{-0.6}^{+0.7}$) oscillatory mode with $\nu_{\max} = 2.21_{-0.12}^{+0.13} \mu\text{Hz}$ (here and throughout we quote the posterior median and the range from the 0.16 to the 0.84 posterior quantile). This is consistent with the presence of a number of unresolved asteroseismic modes in the RV data. The low Q factor in this case refers to the inverse fractional width of the band over which the modes are excited, not the quality of any individual mode. Our posterior for ν_{\max} from this data set is shown in Figure 2.

4.2. SONG Observations

In order to confirm the oscillations detected in the archival data, we used the Hertzprung SONG telescope (Grundahl et al. 2017) to conduct high time cadence follow-up observations. These were carried out in the highest resolution mode ($R \approx 110,000$) with an integration time of 30 s, between 2016 September 27 and 2017 January 12. During this time we attempted to obtain at least one visit per available night, for a total of 254 epochs over the campaign. The spectra were extracted using the SONG pipeline (see Grundahl et al. 2017). SONG employs an iodine cell for precise wavelength calibration, and the velocities were determined using the *iSONG* software following the same procedures as described in Grundahl et al. (2017). The typical velocity precision per visit is 2.5 m s^{-1} , allowing us to easily detect the oscillations that display a peak-to-peak amplitude of $\approx 170 \text{ m s}^{-1}$. Figure 3 displays the RVs obtained—oscillations are easily visible as well as a long-term trend, due to the planetary companion.

¹¹ <https://github.com/farr/Ensemble.jl>; this package implements several stochastic sampling algorithms based on the “stretch move” proposal used in `emcee` (Foreman-Mackey et al. 2013) and introduced in Goodman & Weare (2010).

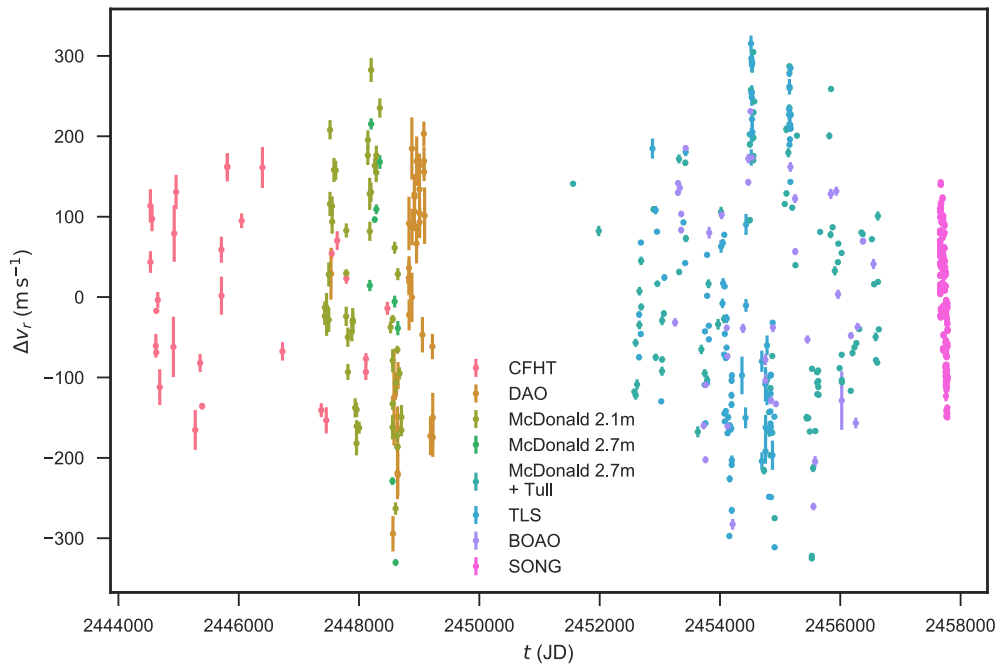


Figure 1. All archival and new radial velocities used for inference in this work. The site and instrument for each data set is indicated in the legend (see the text for a full description). The data used to create this figure are available.

From this data set alone we also find evidence for a low-quality ($Q = 3.1_{-0.8}^{+1.2}$) oscillatory mode with $\nu_{\max} = 2.33_{-0.14}^{+0.13} \mu\text{Hz}$, which is consistent with the inference from the archival data. This posterior is shown in Figure 2.

4.3. K2 Observations

In order to verify the results of the novel analysis presented above, we sought to obtain an independent detection of the oscillations of Aldebaran and compare the frequencies determined with the two methods. Aldebaran was observed with *K2* (Howell et al. 2014), a two-wheeled revival of the *Kepler* Mission (Borucki et al. 2010), under Guest Observer Program 130471 in Campaign 13, from 2017 March 8 to May 27. Aldebaran and similar high-luminosity K giants are well known to show photometric variability due to solar-like oscillations (Bedding 2000), and hence the continuous, high-precision *K2* light curves allow an independent confirmation of our CARMA results.

As Aldebaran is extremely bright, it saturates the *Kepler* detector and it is therefore not possible to use standard photometry pipelines to extract a *K2* light curve. We instead use halo photometry (White et al. 2017), whereby unsaturated pixels from the outer part of the large and complicated halo of scattered light around bright stars are used to reconstruct a light curve as a weighted linear combination of individual pixel-level time series, as described in Appendix B.

Figure 5 shows the light curve and power spectrum of the *K2* observations of Aldebaran. We detect clear variability on an average timescale of ~ 5 days, consistent with the expected timescale for solar-like oscillations for a high-luminosity red giant. To measure global asteroseismic parameters we model the background variability in the Fourier domain using the methodology described in Huber et al. (2009), yielding a frequency of maximum power of $\nu_{\max} = 2.2 \pm 0.25 \mu\text{Hz}$ and amplitude per radial mode of 1850 ± 500 ppm. Due to the

limited frequency resolution of the 70 day *K2* time series we were unable to measure the large frequency separation $\Delta\nu$, which is expected to be $\approx 0.5 \mu\text{Hz}$.

Using the *K2PS* planet-search code (Parviainen et al. 2016; Pope et al. 2016a) to examine this light curve, we search for transits across a wide range of periods, and find no evidence either of short-period planetary transits or an eclipsing stellar companion.

4.4. Planetary and Stellar Parameters

By jointly fitting a Keplerian for the planet with a CARMA model for the stellar oscillations to the combined archival and SONG data sets (Figure 1), we obtain a precise estimate of both ν_{\max} and the planetary orbital parameters. The planetary orbital parameters that we obtain are similar to Hatzes et al. (2015), but with larger uncertainty that is likely due to our more flexible and correlated model for the stellar component of the RV signal: period $P = 629.0_{-2.1}^{+1.7}$ days, eccentricity $e = 0.17 \pm 0.07$; and RV semi-amplitude $K = 127_{-14}^{+15} \text{m s}^{-1}$.

The stellar oscillations are best fit with a single, low-quality ($Q = 2.8_{-0.5}^{+0.6}$) oscillatory mode with $\nu_{\max} = 2.24_{-0.08}^{+0.09} \mu\text{Hz}$. We find no improvement in the marginal likelihood (evidence) or other model-selection information criteria (Gelman et al. 2013) from models with additional oscillatory modes, so we conclude that the large spacing $\Delta\nu$ is not observable in this data set. Figure 4 shows the power spectral density of the radial velocity of Aldebaran inferred from our full data set for frequencies close to ν_{\max} ; the presence of a recognizable peak is clear.

We have used the additional constraint of ν_{\max} determined from this analysis to update the stellar properties of Aldebaran. The details of the stellar modeling are presented in Appendix C. We have considered the impact of our additional ν_{\max} constraint and run our analysis for different sets of spectroscopic estimates. For final values we adopt the Sheffield et al. (2012) spectroscopic solution as being “middle of the

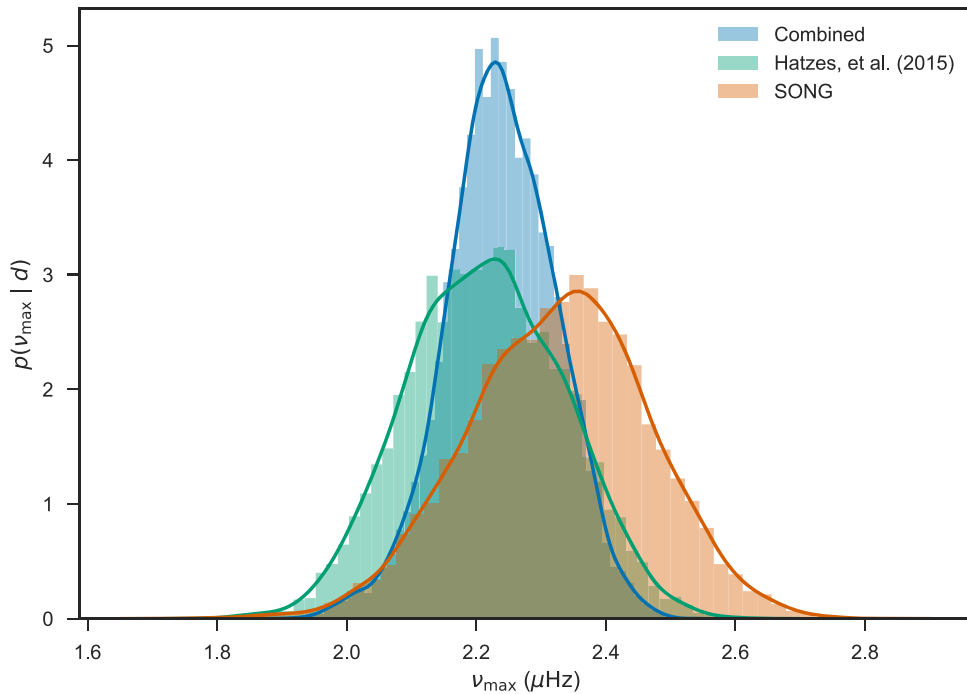


Figure 2. Posterior for ν_{\max} from the complete, combined RV data set described in this paper (blue), the archival data from Hatzes et al. (2015) (green), and the SONG data described in Section 4.2 (red). The inference on the archival data is consistent with the independent inference on the SONG data set alone. The data used to create this figure are available.

road” estimates. For the analysis without constraint on ν_{\max} we find estimates of the stellar properties as $M = 1.27^{+0.24}_{-0.20} M_{\odot}$ and age $4.9^{+3.6}_{-2.0}$ Gyr. This value and uncertainty are consistent with those obtained from other non-asteroseismic analyses of Aldebaran (e.g., Abia et al. 2012; Hatzes et al. 2015). With the inclusion of ν_{\max} we find $M = 1.16 \pm 0.07 M_{\odot}$ and age $6.4^{+1.4}_{-1.1}$ Gyr. It is clear that the addition of ν_{\max} provides substantially more precise estimates of mass and age. With this stellar mass, the RV signal translates to an inclination-dependent planetary mass of $M \sin i = 5.8 \pm 0.7 M_J$ (Torres et al. 2008, Equation (1)), a massive giant planet; for sufficiently high inclinations ($\gtrsim 45^\circ$), the mass of Aldebaran b may exceed $13 M_J$, making it a possible low-mass brown dwarf candidate. A recent study by Hatzes et al. (2018) has cast doubt on the validity of the detection of the massive planet γ Draconis b, and by extension similar planets around similar K giants such as Aldebaran. We remain convinced that the γ Draconis problem is not an issue in this case, and Aldebaran b is a bona-fide planet, for reasons outlined in Appendix D.

With the determination of the stellar mass it is possible to infer the parameters that Aldebaran had while it was on the main sequence. We conduct a Monte Carlo simulation, drawing masses randomly from a Gaussian distribution $M \sim \mathcal{N}(1.16, 0.07)$ and metallicities $[\text{Fe}/\text{H}] \sim \mathcal{N}(-0.15, 0.2)$ (Decin et al. 2003) to predict the luminosity of the main-sequence progenitor, and the semimajor axis of the planet’s orbit. Using the same Rodrigues et al. (2017) MESA models as were used to compute the stellar parameters, interpolating with the ISOCHRONES package (Morton 2015), we compute the evolution of the luminosity L of the star along the main sequence; L evolves from $2.0 \pm 0.7 L_{\odot}$ at 0.5 Gyr to $3.5 \pm 2.3 L_{\odot}$ at 4.5 Gyr. We note that this implies that the planet at a semimajor axis of 1.50 ± 0.03 au would have been

subject to an insolation comparable to that of the Earth, evolving from 0.5 to 3.24 Gyr from 0.82 ± 0.27 to $1.25^{+0.52}_{-0.40}$ times that of the Earth today (Figure 6). After ~ 3.2 Gyr, the high mass tail of the simulations have evolved off of the main sequence and dominate estimates for the insolation, while masses at the low end permit a substantially longer duration on the main sequence (\sim Gyr). Subject as well as this to the great uncertainties of the planet’s orbital evolution and albedo, Aldebaran b and any of its moons (or its S-type planets if it is a brown dwarf, i.e., planets orbiting the brown dwarf and not the primary or wider binary) may well have hosted temperate environments for some of their history, now long-since destroyed by their star’s evolution away from the main sequence.

5. Conclusions

Using sophisticated time-domain CARMA models for the stellar activity in Aldebaran, we have confirmed the previously suspected planet and additionally detected acoustic oscillations that permit a mass determination with a precision of $\sim 6\%$. We have confirmed both of these results with new ground-based observations, and space-based photometry with K2.

From this pilot study with Aldebaran, we have shown that with limited quantities of data of limited quality, we can nevertheless do asteroseismology from the ground and obtain very precise estimates of stellar parameters. Furthermore, improvements in the algorithm may also permit the detection of not only ν_{\max} but also $\Delta\nu$ from similar measurements, permitting more sophisticated asteroseismic analysis. Sufficient RV data either already exist, or are trivial to obtain, in order to do this for essentially all bright giants; while for asteroseismology of solar-like stars, these new methods will allow significantly relaxed observing requirements. One rich archive is the series of observations with the Hamilton Échelle Spectrograph at Lick Observatory, studying

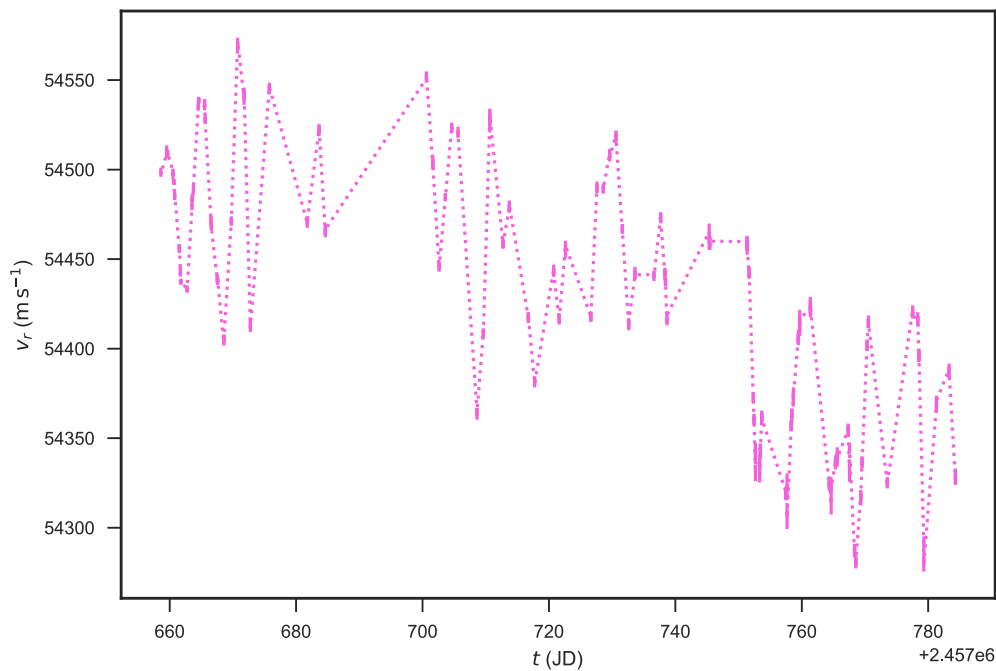


Figure 3. New radial velocities of Aldebaran obtained by the Hertzprung SONG Telescope. Clear oscillations can be seen, plus a trend representing part of the planetary orbit. The data used to create this figure are available.

373 G and K giants (e.g., Frink et al. 2001; Hekker et al. 2006; Ortiz et al. 2016). The method may also be useful in detecting rotational or other periodic variability in the Lick–Carnegie Exoplanet Survey HIRES/Keck Precision Radial Velocity Exoplanet Survey (Butler et al. 2017) of 1624 FGKM dwarfs, although the time sampling is by design too coarse to detect p -mode oscillations in these stars. Furthermore, CARMA models and related methods will enhance deep, all-sky, sparse photometric surveys: an immediate future test of this will be from *Hipparcos*; while only 58 epochs of photometry are available for Aldebaran, at a sampling we find to be insufficient for our purposes, stars at higher latitudes may often have 150–200 epochs and more even sampling (van Leeuwen 1997), and the 14 bright K giants in *Hipparcos* noted by Bedding (2000) are an ideal first test case. This can naturally be extended to *Gaia* in space (Gaia Collaboration et al. 2016), or the Large Synoptic Survey Telescope from the ground (Angel et al. 2000; Tyson & Angel 2001; LSST Science Collaboration et al. 2009), from which many thousands of new asteroseismic determinations will be possible. In future RV surveys, it may be possible to beat the Sato et al. (2005) $\sim 30 \text{ m s}^{-1}$ RV precision limit for red giants by taking many closely spaced observations and modeling-out the effects of stellar oscillations: this will allow us to dig deeper into this intrinsic stellar noise to detect less-massive planets around these stars.

We would like to thank Tim Bedding, David Hogg, and Dan Foreman-Mackey for their helpful discussions. We would like to thank the anonymous referee for their efforts and their comments.

We would like to commend the authors of Hatzes et al. (2015) for making their data publicly available on SIMBAD.

The authors would like to acknowledge the Gadigal people of the Eora Nation on whose ancestral lands the University of

Sydney is built, and we pay our respects their knowledge, and their elders past and present.

B.P. is grateful for funding from the Breakthrough Prize Foundation. This work was performed in part under contract with the Jet Propulsion Laboratory (JPL) funded by NASA through the Sagan Fellowship Program executed by the NASA Exoplanet Science Institute. T.R.W. acknowledges the support of the Villum Foundation (research grant 10118). D.H. acknowledges support by the National Aeronautics and Space Administration under Grants NNX14AB92G, NNX17AF76G, and 80NSSC18K0362 issued through the *Kepler* Participating Scientist Program and the K2 Guest Observer Program.

Funding for the Stellar Astrophysics Centre is provided by the Danish National Research Foundation. This research has made use of the SIMBAD database, operated at CDS, Strasbourg, France, and NASA’s Astrophysics Data System. The *Kepler* data presented in this Letter were obtained from the Mikulski Archive for Space Telescopes (MAST). STScI is operated by the Association of Universities for Research in Astronomy, Inc., under NASA contract NAS5-26555. Support for MAST for non-*HST* data is provided by the NASA Office of Space Science via grant NNX13AC07G and by other grants and contracts.

This work has made use of observations made with the Hertzprung SONG telescope operated on the Spanish Observatorio del Teide on the island of Tenerife by Aarhus and Copenhagen Universities and by the Instituto de Astrofísica de Canarias.

The Villum Foundation, the Danish Council for Independent Research—Natural Sciences and the Carlsberg Foundation are thanked for their support on building the SONG prototype on Tenerife. We thank Jens Jessen-Hansen, Rasmus Handberg, and René Tronsgaard Rasmussen for their contribution to the

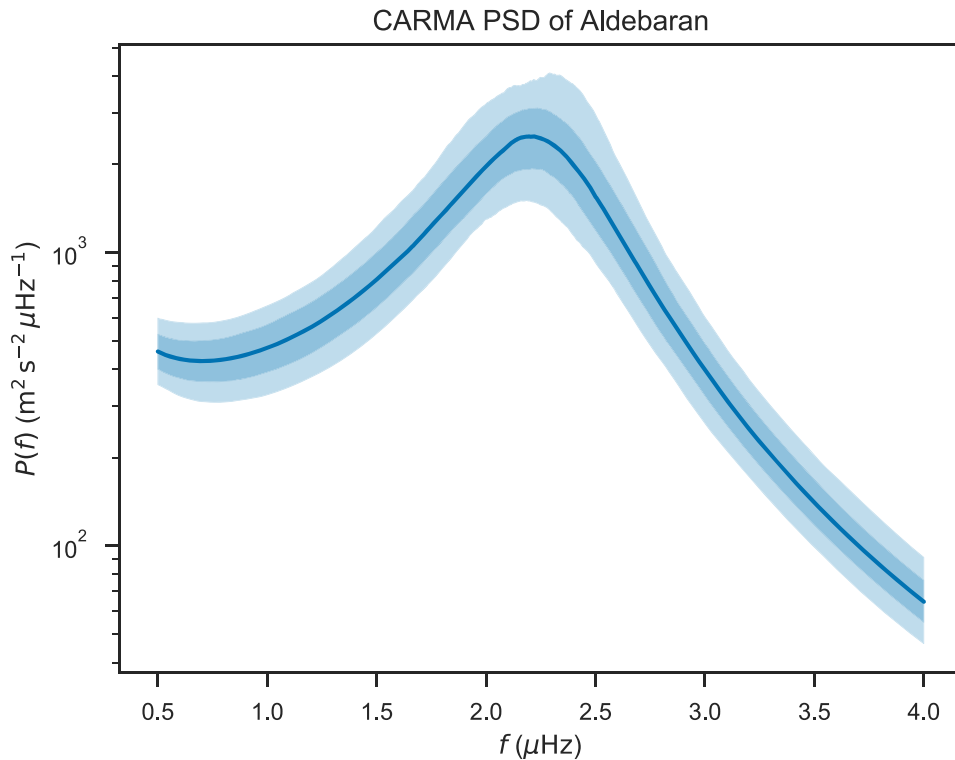


Figure 4. Power spectral density derived from the CARMA analysis of archival and SONG RV observations of Aldebaran, showing the clear peak at around 2 μHz . The dark and light shaded regions represent 1σ and 2σ posterior probability contours. The data used to create this figure are available.

development of the SONG data reduction pipeline and archive system.

W.M.F., G.R.D., T.N., J.W.B., A.M., and M.N.L. are supported in part by the STFC.

Software: IPYTHON (Pérez & Granger 2007), SciPy (Jones et al. 2001), MATPLOTLIB (Hunter 2007), ASTROPY (Astropy Collaboration et al. 2013), NUMPY (Van Der Walt et al. 2011), ISOCHRONES (Morton 2015), JULIA (Bezanson et al. 2017).

The data, code, and LATEX source used to produce this document can be found at <https://github.com/farr/Aldebaran> under an open-source “MIT” license.

Appendix A CARMA Models

A CARMA process corresponds to the solution, $y(t)$, of the stochastic ODE

$$\prod_{i=1}^p \left[\frac{d}{dt} - r_i \right] y(t) = \prod_{j=1}^q \left[\frac{d}{dt} - b_j \right] \eta(t), \quad (5)$$

where $p, q \in \mathbb{Z}$, $p > q \geq 0$ define the order of the process; $r_i \in \mathbb{C}$, $\Re r_i < 0$ are the roots of the characteristic equation of the ODE; $b_j \in \mathbb{C}$, $\Re b_j < 0$ are corresponding roots of the inverse process; and $\eta(t)$ is a white-noise GP with $\langle \eta(t) \rangle = 0$ and $\langle \eta(t)\eta(t') \rangle = \sigma^2 \delta(t - t')$. The constraint that $\Re r_i < 0$ and $\Re b_j < 0$ ensures that the linear operator defining the process and its inverse are invertable. Under the assumption that the solution, $y(t)$, is real, roots r_i and b_j must either be real or occur in complex conjugate pairs. The power spectrum of the

process is

$$P_y(f) = \sigma^2 \left| \frac{\prod_{j=1}^q [2\pi i f - b_j]}{\prod_{i=1}^p [2\pi i f - r_i]} \right|^2. \quad (6)$$

The power spectrum is a rational function of frequency with poles at $2\pi i f = r_i$ and zeros at $2\pi i f = b_j$; because of the invertable constraints, these poles and zeros all occur when $\Im f \neq 0$. The autocorrelation function corresponding to the power spectrum in Equation (6) is

$$\rho_y(\tau) = \langle y(t)y(t + \tau) \rangle = \sum_{i=1}^p A_i^2 e^{r_i \tau}, \quad (7)$$

where the rms amplitudes of the p different modes, A_i , are functions of σ and the values of the roots r_i and b_j . If $q = p - 1$, then the A_i are independent, while if $q < p - 1$ then there are interdependencies among the A_i . From either the power spectrum in Equation (6) or the autocorrelation function in Equation (7), it is apparent that a real root r_i represents an exponentially decaying mode with r_i the rate constant, while a complex conjugate pair of r_i represent an oscillatory mode with decay rate $\Re r_i$ and angular frequency $|\Im r_i|$. Oscillatory modes can also be described by their frequency f and quality factor Q via $r = f/(2Q) \pm 2\pi i f$. Decaying modes generate a damped random walk, also known as a Ornstein–Uhlenbeck process. More discussion of CARMA processes, including formulae for A_i in terms of σ , r_i , and b_j , can be found in Kelly et al. (2014) and references therein.

Our preferred model for the data uses one decaying mode and one oscillatory mode in the CARMA process to capture the

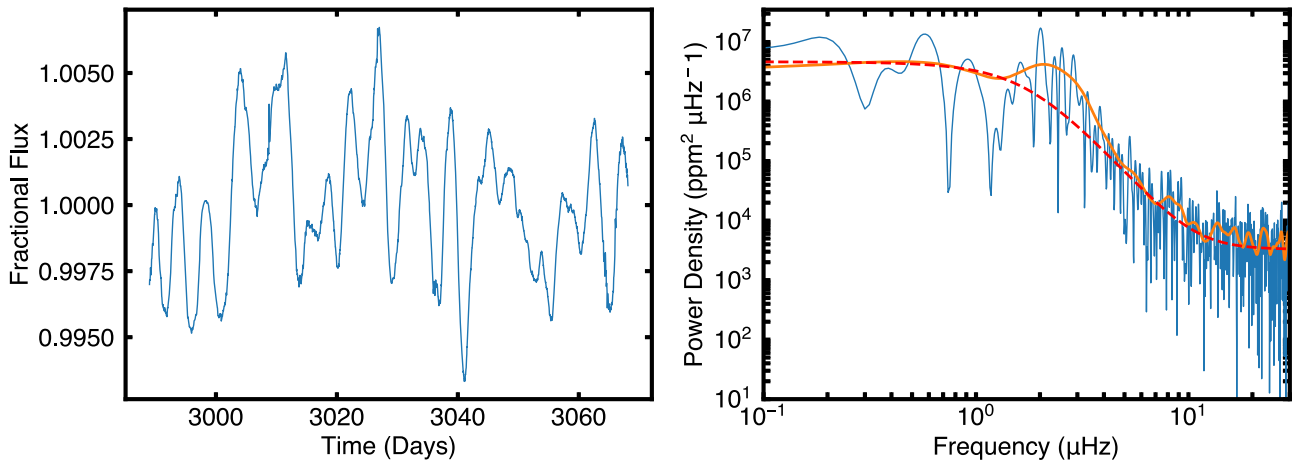


Figure 5. *K2* light curve (left) and power spectrum (right) of Aldebaran. The red dashed line shows the background model, and the orange line is a heavily smoothed version of the power spectrum used to measure the frequency of maximum power.

unresolved superposition of many asteroseismic modes (see Section 4.4); we have fit models with more than one mode of each type, but find no improvement in model-selection criteria from the expanded parameter space. The priors that we impose in all cases on the parameters of the CARMA model, planetary RV signal, and instrumental and site effects are given in Table 1. A draw from the posterior for our canonical model in shown in data space in Figure 7.

The Kalman filter implementation of the CARMA likelihood is not unique. Foreman-Mackey et al. (2017) showed how a dimensional expansion can be used to reduce the standard GP covariance matrix for this same process, with autocorrelation given by Equation (7) under observations at times t_k , to a banded form that can then be Cholesky-decomposed in the standard GP likelihood function in $\mathcal{O}(n)$ time. These “*celerite*” models are formally equivalent to a Kalman CARMA model with $q = p - 1$ and differ only in their computational implementation.

Appendix B Halo Photometry

The *Kepler Space Telescope* (Borucki et al. 2010) suffered a critical reaction wheel failure in 2013 May, which made it impossible to maintain a stable pointing and therefore continue its nominal mission. It was revived as *K2* (Howell et al. 2014), balanced by orienting perpendicular to the Sun. This requires that *K2* observes fields in the Ecliptic in ~ 80 days Campaigns; Aldebaran was observed in Campaign 13.

The *Kepler* detector saturates for stars brighter than the ~ 11 th magnitude. Nevertheless, the excess flux deposited in a saturated pixel spills conservatively up and down the pixel column, such that it is possible to sum this “bleed column” for bright stars and still obtain precise photometry, such as was done for the brightest star in the nominal *Kepler* mission, θ Cyg ($V = 4.48$; Guzik et al. 2011, 2016; White et al. 2013). There are two main reasons why this is not possible for all bright stars in general. First, because the onboard data storage and downlink bandwidth from *Kepler* are limited, it is often not desirable to store and download the large number of pixels that are required for such bright stars. Second, if the bleed column for a sufficiently bright star reaches the edge of the chip, flux spills over and is not conserved, imposing a hard brightness limit that depends on the distance to the detector edge.

Collateral “smear” data, which are collected to help calibrate the photometric bias from stars sharing the same column as a target, can be used to reconstruct light curves for un-downloaded bright stars and thereby avoid bandwidth constraints (Pope et al. 2016b), but these data are still rendered unusable if the bleed column falls off the edge of the chip and contaminates the smear rows.

Bright stars have a wide, complicated, position-dependent point-spread function arising from diffraction and scattering from secondary and higher-order reflections inside the instrument, with the result that they may contaminate thousands of nearby pixels with significant flux. We can therefore use this “halo” of unsaturated pixels for photometry. The brightness of this halo varies in the same way as that of the primary star, and we therefore obtain data in a region of 20-pixel radius around the mean position of Aldebaran, and discard saturated pixels. In this Letter we proceed as in White et al. (2017), in which the method was demonstrated on the seven bright Pleiades, with only minor changes.

The flux f_i at each cadence i is constructed as a weighted sum of pixel values p_{ij} :

$$f_i = \sum_{j=1}^M w_j p_{ij}. \quad (8)$$

We choose the weights w_j such that they lie between 0 and 1, add to unity, and minimize the total variation (TV) of the weighted light curve. In the continuous case, n th order TV is defined as the integral of the absolute value of the n th derivative of a function; in the discrete case, replacing the derivative with finite differences, first-order TV becomes

$$\text{TV} = \frac{\sum_{i=1}^N |f_i - f_{i-1}|}{\sum_{j=1}^N f_j} \quad (9)$$

and likewise second-order TV the equivalent expression in second-order finite differences. The efficacy of this method was recently confirmed by Kallinger & Weiss (2017), comparing BRITe-Constellation observations of Atlas to *K2* halo photometry and finding excellent agreement in the frequency and amplitude of the reported oscillations.

In an improvement since White et al. (2017), we use the AUTOGRAD library (Maclaurin et al. 2015) to calculate analytic derivatives for the TV objective function, which reduces the

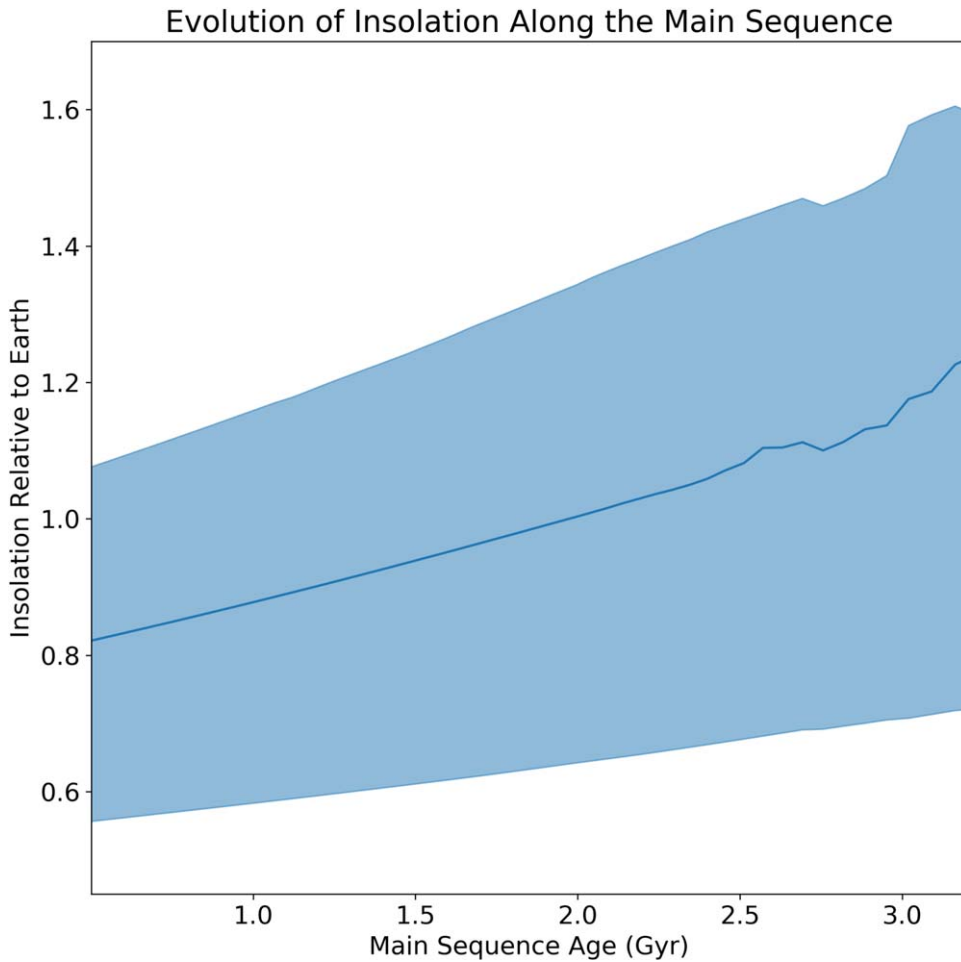


Figure 6. Evolution of the insolation of Aldebaran b relative to the incident sunlight on Earth, as a function of the age of Aldebaran on the main sequence. We end the simulation plot at 3.2 Gyr, as after this, the high tail of the distribution of simulated masses has left the main sequence and disturbs estimates of the insolation. The solid line is the mean of simulations, and the shaded region represents 1σ equivalent deviations. It is likely that Aldebaran b spent some time on the main sequence with an equilibrium temperature similar to Earth.

computational time for a single halo light curve on a commercial laptop from tens of minutes to a few seconds.

As a final step to reduce residual uncorrected systematics, we apply the K2SC (Aigrain et al. 2016) GP-based systematics correction code to the initial halo light curve, but the effect of this in the present case for Aldebaran is minimal. There is somewhat higher than usual residual noise at harmonics of $46 \mu\text{Hz}$ (4 d^{-1} , the satellite thruster firing frequency), but this is nevertheless very small in comparison to the signal from Aldebaran, and may be ascribed to the large fraction of the pixel mask occupied by the bleed column from this extremely bright star.

Appendix C Stellar Modeling

C.1. Stellar Models

We used our determination of ν_{max} and several combinations of the asteroseismic and spectroscopic parameters, along with luminosity, to estimate the fundamental stellar parameters via fitting to stellar models. We used MESA models (Paxton

et al. 2011, 2013) in conjunction with the Bayesian code PARAM (da Silva et al. 2006; Rodrigues et al. 2017). A summary of our selected “benchmark” options is as follows.

1. Medalist scale from Grevesse & Noels (1993b) as described in Rodrigues et al. (2017).
2. Heavy element partitioning from Grevesse & Noels (1993a).
3. OPAL equation of state (Rogers & Nayfonov 2002) along with OPAL opacities (Iglesias & Rogers 1996), with complementary values at low temperatures from Ferguson et al. (2005).
4. Nuclear reaction rates from NACRE (Angulo et al. 1999).
5. The atmosphere model according to Krishna Swamy (1966).
6. The mixing length theory to describe convection (we adopt a solar-calibrated parameter $\alpha_{\text{MLT}} = 1.9657$).
7. Convective overshooting on the main sequence is set to $\alpha_{\text{ov}} = 0.2 H_p$, with H_p the pressure scale height at the border of the convective core. Overshooting was applied according to the Maeder (1975) step function scheme.
8. No rotational mixing or diffusion is included.

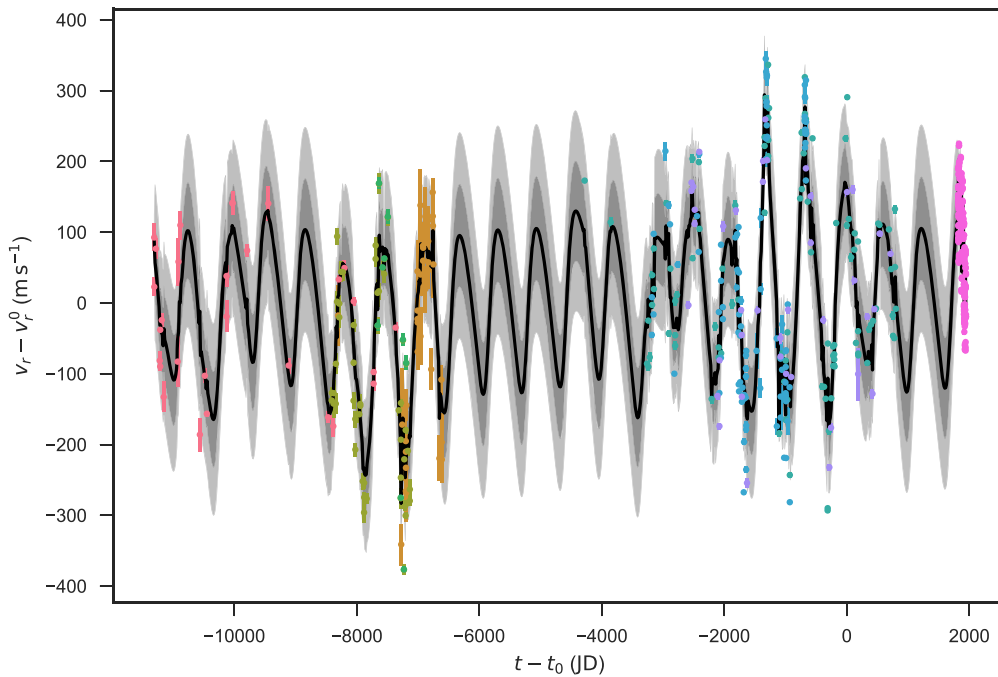


Figure 7. Posterior draw from our model plotted with the observed radial velocities. Each site’s radial velocity has been shifted by the model’s site-specific RV offset and errorbars have been scaled by the model’s site-specific errorbar scaling. Data colors are as in Figure 1. The black line gives the sum of the model’s Keplerian component and the mean of the inferred stochastic component; the dark and light bands give the 1- and 2-sigma uncertainty in the inferred stochastic component. Between observations, the uncertainty in the stochastic component increases; it reduces near observations, as each observation provides some information about the stellar noise that propagates to nearby times because of the temporal correlation in the noise. Stellar oscillations are apparent in the short-timescale wiggles in the stochastic component between nearby observations; there is also a significant long-period correlated component (represented in our model by an exponentially decaying eigenmode). The data used to create this figure are available.

We do not need to correct for the line-of-sight Doppler shift at the frequency precision available in our data (Davies et al. 2014).

C.2. Additional Modeling Inputs

In addition to the asteroseismic parameters, spectroscopically determined temperature and metallicity values are needed. There exist multiple literature values for Aldebaran. We chose to compare a range of literature values to investigate what uncertainty these systematically differing models produce in inferred stellar properties.

To ensure that the values are self-consistent, when a literature value was chosen for temperature, we took the stellar metallicity from the same source i.e., matched pairs of temperature and metallicity. The final constraint is the stellar luminosity, which may be estimated as follows (e.g., see Pijpers 2003):

$$\log_{10} \frac{L}{L_{\odot}} = 4.0 + 0.4M_{\text{bol},\odot} - 2.0 \log_{10} \pi [\text{mas}] - 0.4(V - A_V + BC(V)). \quad (10)$$

The solar bolometric magnitude $M_{\text{bol},\odot} = 4.73$ is taken from Torres (2010), from which we also take the polynomial expression for the bolometric correction $BC(V)$. We assume extinction A_V to be zero.

The final constraint available for Aldebaran is the angular diameter of the star as measured by long baseline interferometry and lunar occultations (20.58 ± 0.03 mas; Beavers & Eitter 1979; Brown et al. 1979; Panek & Leap 1980; Richichi & Roccatagliata

2005), combined with the *Hipparcos* parallax of 19.96 ± 0.38 pc to produce a physical radius constraint of $R_{\text{int}} = 44.2 \pm 0.9 R_{\odot}$.

As Table 2 shows, the spectroscopic parameters of Aldebaran are somewhat unclear, particularly $\log g$ and $[\text{FeH}]$, which may have an impact on the recovered stellar properties when fitting to models. To explore what impact each parameter is having on the final stellar properties, multiple PARAM runs were performed, using different constraints. Two constraints potentially in tension were ν_{max} and the spectroscopically determined $\log g$. ν_{max} has been shown to scale with the stellar $\log g$ (Kjeldsen & Bedding 1995; Belkacem et al. 2011),

$$\frac{\nu_{\text{max}}}{\nu_{\text{max},\odot}} = \frac{\log g}{\log g_{\odot}} \left(\frac{T_{\text{eff}}}{T_{\text{eff},\odot}} \right)^{-1/2}. \quad (11)$$

Using Equation 11 with the values in Table 2 predicts ν_{max} in the range $0.5\text{--}6 \mu\text{Hz}$. Reversing the equation to produce a predicted $\log g$ from the observed $\nu_{\text{max,obs}} = 2.23 \pm 0.1 \mu\text{Hz}$ results in a predicted $\log g \sim 1.2$ dex, using an assumed temperature of 3900 K. The solar calibration values used here are $\log g_{\odot}/(\text{m s}^{-1}) = 2.44$ dex, $\nu_{\text{max},\odot} = 3150 \mu\text{Hz}$ and $T_{\text{eff},\odot} = 5777$ K.

Table 3 shows the results, for all modeling variations, both different inputs and different constraints. It shows that results with the addition of ν_{max} as a constraint exhibit in general smaller uncertainties, with or without the addition of $\log g$ as a constraint.

Recovering the mass without the use of asteroseismic constraints produces considerable scatter on the results

Table 2
Spectroscopic Stellar Parameters from each Literature Source, along with Calculated Luminosity

Spectroscopy Source	T_{eff} (K)	$\log g$ (dex)	[FeH] (dex)	Luminosity (L_{\odot})
Sheffield et al. (2012) _a	3900	1.3	0.17	480
Sheffield et al. (2012) _b	3900	1.3	0.05	480
Prugniel et al. (2011)	3870	1.66	-0.04	507
Massarotti et al. (2008)	3936	1	-0.34	456
Frasca et al. (2009)	3850	0.55	-0.1	526

Note. All temperature uncertainties are assumed to be 50 K, 0.2 dex in $\log g$, and 0.1 dex in [FeH]. For the two Sheffield et al. (2012) results, labeled by *a* and *b*, the reason for the discrepancy between the two sets of metallicity results is not discussed.

Table 3
Recovered Stellar Properties from PARAM Using Various Constraints

Spectroscopy Source	Mass (M_{\odot})	Radius (R_{\odot})	Age (Gyr)
ν_{max} , $\log g$, T_{eff} , R_{int} , L and [FeH]			
Sheffield et al. (2012) _a	1.17 ^{+0.07} _{-0.07}	43.9 ^{+0.9} _{-0.9}	6.5 ^{+1.4} _{-1.1}
Sheffield et al. (2012) _b	1.17 ^{+0.07} _{-0.07}	43.8 ^{+0.8} _{-0.9}	6.4 ^{+1.4} _{-1.1}
Prugniel et al. (2011)	1.17 ^{+0.07} _{-0.07}	43.9 ^{+0.9} _{-0.9}	6.2 ^{+1.4} _{-1.1}
Massarotti et al. (2008)	1.13 ^{+0.07} _{-0.07}	43.5 ^{+0.9} _{-0.9}	6.0 ^{+1.4} _{-1.1}
Frasca et al. (2009)	1.02 ^{+0.04} _{-0.04}	44.0 ^{+0.8} _{-0.8}	10.3 ^{+1.5} _{-1.4}
$\log g$, T_{eff} , R_{int} , L and [FeH]			
Sheffield et al. (2012) _a	1.43 ^{+0.26} _{-0.24}	43.8 ^{+0.9} _{-0.9}	3.5 ^{+2.7} _{-1.4}
Sheffield et al. (2012) _b	1.27 ^{+0.24} _{-0.2}	43.8 ^{+0.9} _{-0.9}	4.9 ^{+3.6} _{-2.0}
Prugniel et al. (2011)	1.25 ^{+0.22} _{-0.19}	43.8 ^{+0.9} _{-0.9}	5.0 ^{+3.5} _{-2.0}
Massarotti et al. (2008)	0.95 ^{+0.11} _{-0.05}	43.8 ^{+0.9} _{-0.9}	10.2 ^{+2.4} _{-3.1}
Frasca et al. (2009)	0.96 ^{+0.04} _{-0.04}	44.4 ^{+0.8} _{-0.8}	11.6 ^{+1.8} _{-1.8}
ν_{max} , T_{eff} , R_{int} , L and [FeH]			
Sheffield et al. (2012) _a	1.17 ^{+0.07} _{-0.07}	43.9 ^{+0.9} _{-0.9}	6.5 ^{+1.4} _{-1.1}
Sheffield et al. (2012) _b	1.16 ^{+0.07} _{-0.07}	43.8 ^{+0.8} _{-0.9}	6.4 ^{+1.4} _{-1.1}
Prugniel et al. (2011)	1.16 ^{+0.07} _{-0.07}	43.9 ^{+0.9} _{-0.9}	6.4 ^{+1.5} _{-1.2}
Massarotti et al. (2008)	1.13 ^{+0.07} _{-0.07}	43.5 ^{+0.9} _{-0.9}	5.9 ^{+1.4} _{-1.0}
Frasca et al. (2009)	1.15 ^{+0.07} _{-0.07}	43.9 ^{+0.9} _{-0.8}	6.5 ^{+1.5} _{-1.2}

Note. Uncertainties quoted are the 68% credible interval. Labels *a* and *b* refer to the different metallicity results from Sheffield, et al. (2012); see Table 2.

(0.96–1.5 M_{\odot}), while the use of asteroseismology brings the mass estimates into closer agreement with one another, with the exception of the very low metallicity solution of Massarotti et al. (2008). Any systematic offset between asteroseismic masses and spectroscopic masses is sensitive to chosen reference mass, in agreement with North et al. (2017).

We have also investigated running PARAM and relaxing one or more constraints. Between runs with and without the luminosity constraint, the average absolute mass offset between the two sets of results was $<0.04 M_{\odot}$ if we also ignore the ν_{max} constraint, and $<0.02 M_{\odot}$ including the ν_{max} .

Appendix D The γ Draconis Problem is Not a Problem

γ Draconis (also known as Eltanin, or γ Dra) is a second-magnitude K5III giant that had been observed by Hatzes & Cochran (1993) as part of the same campaign that led to the discovery of Aldebaran b and Pollux b. Hatzes et al. (2018, p. 10) have recently shown that the 702 days period RV variations of the putative Eltanin b disappeared from 2011 to

2013, returning in 2014 with a different amplitude and phase. They ascribe this to a previously unidentified kind of stellar variability, and warn that “given that the periods found in α Tau [Aldebaran] are comparable to those in γ Dra and both stars are evolved with large radii, a closer scrutiny of the RV variability of α Tau is warranted.”

For several reasons, we are not convinced that this poses an issue for Aldebaran or for K giant RV planets more generally. Hatzes et al. (2018) suggested that the new type of stellar variability may be oscillatory convective modes, but both Aldebaran and Eltanin have much lower luminosities and longer periods than would seem to be allowed by the period–luminosity relation predicted for these otherwise unobserved modes (Saio et al. 2015; Hatzes et al. 2018, Figure 9). If these are identified with the long secondary periods (LSPs) observed in some bright red giants ($L \approx 1000 L_{\odot}$), then Aldebaran and Eltanin are both too faint, and lack the mid-infrared excess typical of LSP stars (Wood & Nicholls 2009). It would also be surprising if the shape of the RV curve could reproduce the harmonic structure of an eccentric Keplerian such as in Aldebaran b ($e = 0.17 \pm 0.07$), let alone the much higher eccentricities observed in other giants (e.g., ι Dra b, $e = 0.7$; Frink et al. 2002).

It would be a cruel conspiracy of nature if red giants support a type of oscillation that is common and closely resembles a planetary signal. We believe this cannot be the case: the populations of planets around subgiants and giants evolved from intermediate-mass stars are similar (Jones et al. 2014), as expected if subgiants evolve into giants and retain their planetary systems, and with very different stellar structures subgiants and giants are unlikely to share modes of long-period pulsation. The similarity of distributions of systems hosted by subgiant and giants could not be reproduced if a large fraction of the giants’ planets were false positives. Moreover, giant planets are expected to be common around intermediate-mass stars (Kennedy & Kenyon 2008), and some are definitely known to be bona-fide planets because they transit their star (e.g., Lillo-Box et al. 2014; Ortiz et al. 2015; Grunblatt et al. 2016, 2017).

We therefore believe that either Eltanin b is not a false positive, or if it is, that it is not a common type of false positive, and is unlikely to affect our certainty that Aldebaran b is real. Hatzes et al. (2018) offered an alternative to the pulsation hypothesis, namely beating between the stellar rotation and the planetary signal; this does not seem implausible.

ORCID iDs

Will M. Farr  <https://orcid.org/0000-0003-1540-8562>
Benjamin J. S. Pope  <https://orcid.org/0000-0003-2595-9114>

Guy R. Davies <https://orcid.org/0000-0002-4290-7351>
 Timothy R. White <https://orcid.org/0000-0002-6980-3392>
 Andrea Miglio <https://orcid.org/0000-0001-5998-8533>
 Mikkel N. Lund <https://orcid.org/0000-0001-9214-5642>
 Victoria Antoci <https://orcid.org/0000-0002-0865-3650>
 Frank Grundahl <https://orcid.org/0000-0002-8736-1639>

References

- Abia, C., Palmerini, S., Busso, M., & Cristallo, S. 2012, *A&A*, **548**, A55
 Aigrain, S., Parviainen, H., & Pope, B. J. S. 2016, *MNRAS*, **459**, 2408
 Angel, R., Lesser, M., Sarlot, R., & Dunham, E. 2000, in ASP Conf. Ser. 195, *Imaging the Universe in Three Dimensions*, ed. W. van Breugel & J. Bland-Hawthorn (San Francisco, CA: ASP), 81
 Angulo, C., Arnould, M., Rayet, G., et al. 1999, *NuPhA*, **656**, 3
 Astropy Collaboration, Robitaille, T. P., Tollerud, E. J., et al. 2013, *A&A*, **558**, A33
 Beavers, W. I., & Eitter, J. 1979, *ApJL*, **228**, L111
 Bedding, T. R. 2000, in The Third MONS Workshop: Science Preparation and Target Selection, ed. T. Teixeira & T. Bedding (Aarhus: Aarhus Univ.), 97
 Belkacem, K., Goupil, M. J., Dupret, M. A., et al. 2011, *A&A*, **530**, A142
 Bezanson, J., Edelman, A., Karpinski, S., & Shah, V. B. 2017, *SIAMR*, **59**, 65
 Borucki, W. J., Koch, D., Basri, G., et al. 2010, *Sci*, **327**, 977
 Brewer, B. J., & Stello, D. 2009, *MNRAS*, **395**, 2226
 Brown, A., Bunclark, P. S., Stapleton, J. R., & Stewart, G. C. 1979, *MNRAS*, **187**, 753
 Butler, R. P., Vogt, S. S., Laughlin, G., et al. 2017, *AJ*, **153**, 208
 Chaplin, W. J., & Miglio, A. 2013, *ARA&A*, **51**, 353
 da Silva, L., Girardi, L., Pasquini, L., et al. 2006, *A&A*, **458**, 609
 Davies, G. R., Handberg, R., Miglio, A., et al. 2014, *MNRAS*, **445**, L94
 Davies, G. R., & Miglio, A. 2016, *AN*, **337**, 774
 Decin, L., Vandenbussche, B., Waelkens, C., et al. 2003, *A&A*, **400**, 709
 Ferguson, J. W., Alexander, D. R., Allard, F., et al. 2005, *ApJ*, **623**, 585
 Foreman-Mackey, D., Agol, E., Ambikasaran, S., & Angus, R. 2017, arXiv:1703.09710
 Foreman-Mackey, D., Hogg, D. W., Lang, D., & Goodman, J. 2013, *PASP*, **125**, 306
 Frasca, A., Covino, E., Spezzi, L., et al. 2009, *A&A*, **508**, 1313
 Frink, S., Mitchell, D. S., Quirrenbach, A., et al. 2002, *ApJ*, **576**, 478
 Frink, S., Quirrenbach, A., Fischer, D., Röser, S., & Schilbach, E. 2001, *PASP*, **113**, 173
 Gaia Collaboration, Prusti, T., de Bruijne, J. H. J., et al. 2016, *A&A*, **595**, A1
 Gelman, A., Hwang, J., & Vehtari, A. 2013, arXiv:1307.5928
 Goodman, J., & Weare, J. 2010, *Communications in Applied Mathematics and Computational Science*, **5**, 65
 Grevesse, N., & Noels, A. 1993a, *PhST*, **47**, 133
 Grevesse, N., & Noels, A. 1993b, in Cours de perfectionnement de l'Association Vaudoise des Chercheurs en Physique 35, La Formation des 'elements Chimiques, AVCP, ed. R. D. Hauck & B. Paltani S. (Lausanne: EPFL), 205
 Grunblatt, S. K., Huber, D., Gaidos, E., et al. 2017, *AJ*, **154**, 254
 Grunblatt, S. K., Huber, D., Gaidos, E. J., et al. 2016, *AJ*, **152**, 185
 Grundahl, F., Fredslund Andersen, M., Christensen-Dalsgaard, J., et al. 2017, *ApJ*, **836**, 142
 Guzik, J. A., Houdek, G., Chaplin, W. J., et al. 2011, arXiv:1110.2120
 Guzik, J. A., Houdek, G., Chaplin, W. J., et al. 2016, *ApJ*, **831**, 17
 Han, I., Lee, B.-C., Kim, K.-M., & Mkrichian, D. E. 2008, *JKAS*, **41**, 59
 Hatzes, A. P., & Cochran, W. D. 1993, *ApJ*, **413**, 339
 Hatzes, A. P., & Cochran, W. D. 1998, *MNRAS*, **293**, 469
 Hatzes, A. P., Cochran, W. D., Endl, M., et al. 2006, *A&A*, **457**, 335
 Hatzes, A. P., Cochran, W. D., Endl, M., et al. 2015, *A&A*, **580**, A31
 Hatzes, A. P., Endl, M., Cochran, W. D., et al. 2018, arXiv:1801.05239
 Haywood, R. D., Collier Cameron, A., Queloz, D., et al. 2014, *MNRAS*, **443**, 2517
 Hekker, S., & Christensen-Dalsgaard, J. 2017, *A&ARv*, **25**, 1
 Hekker, S., Reffert, S., Quirrenbach, A., et al. 2006, *A&A*, **454**, 943
 Howell, S. B., Sobeck, C., Haas, M., et al. 2014, *PASP*, **126**, 398
 Huber, D., Stello, D., Bedding, T. R., et al. 2009, *CoAst*, **160**, 74
 Huber, D., Zinn, J., Bojsen-Hansen, M., et al. 2017, *ApJ*, **844**, 102
 Hunter, J. D. 2007, *CSE*, **9**, 90
 Iglesias, C. A., & Rogers, F. J. 1996, *ApJ*, **464**, 943
 Jones, E., Oliphant, T., Peterson, P., et al. 2001, SciPy: Open Source Scientific Tools for Python, <http://www.scipy.org/>
 Jones, M. I., Jenkins, J. S., Bluhm, P., Rojo, P., & Melo, C. H. F. 2014, *A&A*, **566**, A113
 Kallinger, T., & Weiss, W. W. 2017, arXiv:1711.02570
 Kelly, B. C., Becker, A. C., Sobolewska, M., Siemiginowska, A., & Uttley, P. 2014, *ApJ*, **788**, 33
 Kennedy, G. M., & Kenyon, S. J. 2008, *ApJ*, **673**, 502
 Kjeldsen, H., & Bedding, T. R. 1995, *A&A*, **293**, arXiv:astro-ph/9403015
 Krishna Swamy, K. S. 1966, *ApJ*, **145**, 174
 Lillo-Box, J., Barrado, D., Moya, A., et al. 2014, *A&A*, **562**, A109
 Lomb, N. R. 1976, *Ap&SS*, **39**, 447
 LST Science Collaboration, Abell, P. A., Allison, J., et al. 2009, arXiv:0912.0201
 Maclaurin, D., Duvenaud, D., & Adams, R. P. 2015, ICML 2015 AutoML Workshop, </bib/maclaurin/maclaurin-autograd/automl-short.pdf>, <https://indico.lal.in2p3.fr/event/2914/session/1/contribution/6/3/material/paper/0.pdf>, <https://github.com/HIPS/autograd>
 Maeder, A. 1975, *A&A*, **40**, 303
 Massarotti, A., Latham, D. W., Stefanik, R. P., & Fogel, J. 2008, *AJ*, **135**, 209
 Mayor, M., & Queloz, D. 1995, *Natur*, **378**, 355
 Morton, T. D. 2015, Isochrones: Stellar Model Grid Package, Astrophysics Source Code Library, ascl:1503.010
 Mosser, B., Belkacem, K., Goupil, M. J., et al. 2011, *A&A*, **525**, L9
 Mosser, B., Dziembowski, W. A., Belkacem, K., et al. 2013, *A&A*, **559**, A137
 North, T. S. H., Campante, T. L., Miglio, A., et al. 2017, arXiv:1708.00716
 Ortiz, M., Gandolfi, D., Reffert, S., et al. 2015, *A&A*, **573**, L6
 Ortiz, M., Reffert, S., Trifonov, T., et al. 2016, *A&A*, **595**, A55
 Panek, R. J., & Leap, J. L. 1980, *AJ*, **85**, 47
 Parviainen, H., Pope, B., & Aigrain, S. 2016, K2PS: K2 Planet Search, Astrophysics Source Code Library, ascl:1607.010
 Paxton, B., Bildsten, L., Dotter, A., et al. 2011, *ApJS*, **192**, 3
 Paxton, B., Cantiello, M., Arras, P., et al. 2013, *ApJS*, **208**, 4
 Pérez, F., & Granger, B. E. 2007, *CSE*, **9**, 21
 Pijpers, F. P. 2003, *A&A*, **400**, 241
 Pope, B. J. S., Parviainen, H., & Aigrain, S. 2016a, *MNRAS*, **461**, 3399
 Pope, B. J. S., White, T. R., Huber, D., et al. 2016b, *MNRAS*, **455**, L36
 Prugniel, P., Vauglin, I., & Koleva, M. 2011, *A&A*, **531**, A165
 Rajpaul, V., Aigrain, S., Osborne, M. A., Reece, S., & Roberts, S. 2015, *MNRAS*, **452**, 2269
 Richichi, A., & Roccatagliata, V. 2005, *A&A*, **433**, 305
 Rodrigues, T. S., Bossini, D., Miglio, A., et al. 2017, *MNRAS*, **467**, 1433
 Rogers, F. J., & Nayfonov, A. 2002, *ApJ*, **576**, 1064
 Saio, H., Wood, P. R., Takayama, M., & Ita, Y. 2015, *MNRAS*, **452**, 3863
 Sato, B., Kambe, E., Takeda, Y., et al. 2005, *PASJ*, **57**, 97
 Scargle, J. D. 1982, *ApJ*, **263**, 835
 Sheffield, A. A., Majewski, S. R., Johnston, K. V., et al. 2012, *ApJ*, **761**, 161
 Stello, D., Huber, D., Grundahl, F., et al. 2017, *MNRAS*, **472**, 4110
 Struve, O. 1952, *Obs*, **72**, 199
 Torres, G. 2010, *AJ*, **140**, 1158
 Torres, G., Winn, J. N., & Holman, M. J. 2008, *ApJ*, **677**, 1324
 Tyson, A., & Angel, R. 2001, in ASP Conf. Ser. 232, The New Era of Wide Field Astronomy, ed. R. Clowes, A. Adamson, & G. Bromage (San Francisco, CA: ASP), 347
 Van Der Walt, S., Colbert, S. C., & Varoquaux, G. 2011, *CSE*, **13**, 22
 van Leeuwen, F. 1997, in Hipparcos Venice 97, ed. B. Battrick & M. A. C. Perryman (Noordwijk: ESA), 19
 van Leeuwen, F. 2007, *A&A*, **474**, 653
 Viani, L. S., Basu, S., Chaplin, W. J., Davies, G. R., & Elsworth, Y. 2017, *ApJ*, **843**, 11
 White, T. R., Huber, D., Maestro, V., et al. 2013, *MNRAS*, **433**, 1262
 White, T. R., Pope, B. J. S., Antoci, V., et al. 2017, *MNRAS*, **471**, 2882
 Wood, P. R., & Nicholls, C. P. 2009, *ApJ*, **707**, 573
 Zinn, J. C., Pinsonneault, M. H., Huber, D., & Stello, D. 2018, arXiv:1805.02650